

## RESEARCH ARTICLE

10.1002/2015JD023547

## Key Points:

- For a unit increase of AOD the height of rain initiation increases by ~5.5 km
- AOD can be enhanced by aerosol upward transport and detrainment through clouds
- Cloud self-shadowing causes overestimated drop size in nonbackscatter angles

## Correspondence to:

D. Rosenfeld,  
daniel.rosenfeld@huji.ac.il

## Citation:

Zhu, Y., D. Rosenfeld, X. Yu, and Z. Li (2015), Separating aerosol microphysical effects and satellite measurement artifacts of the relationships between warm rain onset height and aerosol optical depth, *J. Geophys. Res. Atmos.*, 120, 7726–7736, doi:10.1002/2015JD023547.

Received 24 APR 2015

Accepted 13 JUL 2015

Accepted article online 16 JUL 2015

Published online 7 AUG 2015

## Separating aerosol microphysical effects and satellite measurement artifacts of the relationships between warm rain onset height and aerosol optical depth

Yannian Zhu<sup>1</sup>, Daniel Rosenfeld<sup>2</sup>, Xing Yu<sup>1</sup>, and Zhanqing Li<sup>3,4</sup>

<sup>1</sup>Meteorological Institute of Shaanxi Province, Xi'an, China, <sup>2</sup>Institute of Earth Sciences, Hebrew University of Jerusalem, Jerusalem, Israel, <sup>3</sup>State Laboratory of Earth Surface Process and Resource Ecology, GCESS, Beijing Normal University, Beijing, China, <sup>4</sup>Department of Atmospheric and Oceanic Science and Earth System Science Interdisciplinary Center, University of Maryland, College Park, Maryland, USA

**Abstract** The high resolution (375 m) of the Visible Infrared Imaging Radiometer Suite on board the Suomi National Polar-Orbiting Partnership satellite allows retrieving relatively accurately the vertical evolution of convective cloud drop effective radius ( $r_e$ ) with height or temperature. A tight relationship is found over SE Asia and the adjacent seas during summer between the cloud-free aerosol optical depth (AOD) and the cloud thickness required for the initiation of warm rain, as represented by the satellite-retrieved cloud droplet  $r_e$  of 14  $\mu\text{m}$ , for a subset of conditions that minimize measurement artifacts. This cloud depth ( $\Delta T_{14}$ ) is parameterized as the difference between the cloud base temperature and the temperature at the height where  $r_e$  exceeds 14  $\mu\text{m}$  ( $T_{14}$ ). For a unit increase of AOD, the height of rain initiation is increased by about 5.5 km. The concern of data artifacts due to the increase in AOD near clouds was mitigated by selecting only scenes with cloud fraction (CF) < 0.1. For CF > 0.1 and  $\Delta T_{14} > \sim 20^\circ\text{C}$ , the increase of  $\Delta T_{14}$  gradually levels off with further increase of AOD, possibly because the AOD is enhanced by aerosol upward transport and detrainment through the clouds below the  $T_{14}$  isotherm. The bias in the retrieved  $r_e$  due to the different geometries of solar illumination was also quantified. It was shown that the retrievals are valid only for backscatter views or when avoiding scenes with significant amount of cloud self-shadowing. These artifacts might have contributed to past reported relationships between cloud properties and AOD.

### 1. Introduction

Aerosols serve as cloud condensation nuclei (CCN) for cloud droplets and can increase cloud albedo and amount and modify cloud microphysics and precipitation formation [Andreae *et al.*, 2004; Andreae and Rosenfeld, 2008; Rosenfeld *et al.*, 2008a; Freud and Rosenfeld, 2012]. The number of CCN activated into cloud droplets is the fundamental microphysical property of a convective cloud. This is because it determines the rate of droplet growth with cloud thickness and conversion into precipitation-size particles [Freud *et al.*, 2011; Rosenfeld *et al.*, 2014a]. The dynamic response of a cloud to changes in CCN and precipitation affects its radiative properties as well [Yan *et al.*, 2014]. The geometry of deep convective clouds may also vary considerably with surface aerosol concentration [Li *et al.*, 2011]. An opposite effect, i.e., an acceleration in the development of precipitation, can occur in clouds ingesting giant CCN, which initiates rain from initial large drops that fall and grow by the collection of much smaller drops [Feingold *et al.*, 1999; Posselt and Lohmann, 2008].

Many studies have reported that aerosols modify rainfall intensity, amount, and spatial and temporal distribution in various ways due to aerosols' radiative and cloud microphysical effects [Tao *et al.*, 2012]. Some studies suggest a decrease in rain rate from convective clouds [Rosenfeld, 2000; Teller and Levin, 2006; Jiang *et al.*, 2008], while others show rain enhancement [Lin *et al.*, 2006; Martins *et al.*, 2009] or no clear effect [Jones and Christopher, 2010]. Koren *et al.* [2012] and Rosenfeld *et al.* [2012], for example, studied aerosol loading and changes in precipitation by analyzing aerosol optical depth (AOD) and rain intensity. Koren *et al.* [2012] found a clear increase in rain intensity with increasing AOD when AOD < 0.3, and Rosenfeld *et al.* [2012] provided a theoretical basis for that observational finding.

Based on satellite-retrieved cloud droplet effective radii ( $r_e$ ), ground-based radar measurements, and Tropical Rainfall Measuring Mission observations,  $r_e$  ranging from 12 to 14  $\mu\text{m}$  appear to be the threshold for initiating

warm rain [Rosenfeld and Gutman, 1994; Rosenfeld, 1999; Rosenfeld and Woodley, 2003; Suzuki et al., 2010; Rosenfeld et al., 2012]. Freud and Rosenfeld [2012] have shown that the conversion rate of cloud droplets into raindrops is proportional to  $r_e^{4.8}$ , which explains previous observations of the strong dependence of cloud top  $r_e$  on rain initiation. Aircraft measurements over the Amazon have revealed that when  $r_e$  exceeds 14  $\mu\text{m}$ , cloud droplets grow big enough to start coalescence and initiate warm rain [Andreae et al., 2004]. Heavy smoke from forest fires in the Amazon reduced cloud droplet sizes and delayed the onset of precipitation from 1.5 km above the cloud base in pristine clouds to more than 5 km above the cloud base in smoky clouds [Rosenfeld, 1999; Konwar et al., 2012]. Aircraft measurements of CCN and cloud microstructure at various altitudes have also been conducted over India. Measurements show a positive relationship between cloud droplet number concentration ( $N_a$ ) and warm rain depth with  $R^2 = 0.79$  [Konwar et al., 2012].

Freud and Rosenfeld [2012] have used a simple adiabatic parcel model where droplets grow exclusively by diffusion to show that the sensitivity of the cloud thickness for reaching a given cloud droplet effective radius ( $D_p$ ) changes almost linearly with  $N_a$ . The parameter  $D_p$  was coined by Freud and Rosenfeld [2012] as the required cloud depth for precipitation initiation. This has been confirmed observationally in winter extratropical cyclones over Israel and in Indian monsoon deep convective clouds where increasing  $N_a$  by 100 per mg of air resulted in an increase of  $\sim 280$  m in the required  $D_p$ .

Zhu et al. [2014] have shown that cloud base temperatures ( $T_{\text{base}}$ ) can be estimated from the Visible Infrared Imaging Radiometer Suite (VIIRS) imager during its early afternoon overpass with a standard error of 1.1°C over the U.S. Department of Energy's Atmospheric System Research Southern Great Plains site. Retrieving  $T_{\text{base}}$  allows retrieving  $D_p$  from satellite measurements, here represents by temperature in this study. Section 2 describes the data and the methodology used to calculate the depth where warm rain initiates. Results from cases selected in the summers of 2012 and 2013 are presented in section 3. The sensitivity to measurement artifacts is discussed in section 4, and a discussion with respect to cause and effects of the found relationship is presented in section 5. A summary is given in section 6.

## 2. Data and Methodology

The Suomi National Polar-Orbiting Partnership, which was launched on 28 October 2011, inaugurated a new generation of operational U.S. polar-orbiting satellites. Its primary imaging instrument is the VIIRS. The VIIRS imager has a basic resolution of 750 m and a subset of channels with a resolution of 375 m at nadir. The vertical evolution of cloud microstructure was constructed by composing the retrieved temperature ( $T$ ) and effective radius ( $r_e$ ) of the tops of a cluster of convective clouds reaching various heights [Rosenfeld and Lensky, 1998]. Due to the validity of exchangeability in time and space, the vertical evolution with time of the  $T$ - $r_e$  relationships of a single convective cloud is similar to a  $T$ - $r_e$  relationship that is composed from a snap shot of a cluster of convective clouds with tops at different heights and temperatures [Lensky and Rosenfeld, 2006]. Retrieving  $T$  and  $r_e$  requires the usage of the brightness temperature difference (BTD) between the bands of 10.8  $\mu\text{m}$  and 12.0  $\mu\text{m}$  for water vapor correction, but these channels are not available at the imager resolution. Rosenfeld et al. [2014b] developed an algorithm to calculate the BTD for the imager resolution and applied it to water vapor correction of the imager 11.5  $\mu\text{m}$  brightness temperature according the formulation of Sullivan et al. [1993]. This provided the basis for calculating  $r_e$  for the imager resolution and further to retrieving cloud microphysical properties, such as the  $T$ - $r_e$  relationship. Here  $T$  is given by the 11.5  $\mu\text{m}$  brightness temperature, and the  $r_e$  is approximated by the 3.7  $\mu\text{m}$  solar reflectance component. The resolution is improved by a factor of 3 relative to other satellite sensors such as the Moderate Resolution Imaging Spectroradiometer (MODIS) or the advanced very high resolution radiometer. Since  $T_{\text{base}}$  is defined as the warmest cloudy pixel, Zhu et al. [2014] developed a methodology to screening cloudy pixels that are suspected to be contaminated by surface radiation by identifying the thermal contrast between adjacent pixels. Retrievals of  $T_{\text{base}}$  and  $r_e$  allow for the development of more accurate  $T$ - $r_e$  relationships for convective clouds [Rosenfeld et al., 2014a].

### 2.1. Data

VIIRS images of convective clouds that are not obscured by higher clouds were selected over Southeast Asia for the months of July and August of 2012 and 2013. The satellite overpass time is  $\sim 13:30$  solar time. At that

time, convection is developing, but extensive anvils are not yet formed. To maximize the quality of the data, all cases must satisfy the following criteria: (1) the convective cloud clusters chosen must not be obscured by higher clouds, (2) the selected cloud clusters must have  $T_{\text{base}} \geq 15^\circ\text{C}$  so that large vertical distance can occur between cloud base and the freezing level, (3) the cloud clusters must have a wide range of cloud top temperatures ( $T_{\text{top}}$ ) so that a fully representative  $T$ - $r_e$  relationship can be established, (4) the largest cloud top  $r_e$  should be at least  $14\ \mu\text{m}$  so that the height for rain initiation can be documented, and (5) the selected cloud clusters must have developed over an area which has enough cloud gaps to allow for the retrieval of AOD. (6) A full representation of cloud tops at all temperatures from cloud base to above the height of precipitation initiation must exist. The area of the rectangle varied to fully cover such convective clusters whose sizes range from  $20 \times 20\ \text{km}^2$  to  $100 \times 100\ \text{km}^2$ .

Coincident measurements of AOD are taken from the daily level-3 MODIS AOD product because of its accessibility and large heritage with other papers, which has a spatial resolution of  $1^\circ \times 1^\circ$ . Additionally, the clouds must not be located where there is a strong gradient in AOD which means that the selected cloud clusters must be located in the area which has nearly the same value of AOD. This will avoid ambiguity when it comes to relating AOD to cloud properties. Sixty-four cases meeting these requirements were identified. The locations of these cases and their mean AOD are shown in Figure 1.

The number of cases corresponding to high AOD is small. In general, convective clouds are not present when AOD is very large. Also, when the cloud fraction (CF) is large, AOD retrievals are not very accurate.

## 2.2. Calculation of the Critical Depth Where Warm Rain Initiates

*Freud and Rosenfeld* [2012] have shown examples of  $r_e$  profiles in four deep convective clouds from four different aircraft field campaigns, representing varying locations, seasons, atmospheric thermodynamic conditions, and aerosol properties. The aircraft-measured vertical profiles show a tight relationship between  $r_e$  and  $D_p$ . The definition of the onset of the warm rain process in this study is when satellite-retrieved  $r_e$  reaches  $14\ \mu\text{m}$ , because this is the  $r_e$  above which the probability for rain becomes very high. Applying the method of *Rosenfeld and Lensky* [1998] to VIIRS imager data, microphysics red-green-blue (RGB) composites and  $T$ - $r_e$  plots for a convective cloud ensemble in an area that contains growing convective clouds were obtained [*Rosenfeld et al.*, 2014b]. The steps followed to estimate  $T_{\text{base}}$  and  $\Delta T_{14}$  are (1) obtain the  $T$ - $r_e$  relation for each convective cloud cluster identified using VIIRS data, (2) estimate  $T_{\text{base}}$  from the  $T$ - $r_e$  relationship as done by *Zhu et al.* [2014], (3) estimate the temperature at the height where  $r_e$  exceeds  $14\ \mu\text{m}$  ( $T_{14}$ ) from the  $T$ - $r_e$  relationship, (4) calculate the temperature difference  $\Delta T_{14}$  between  $T_{\text{base}}$  and  $T_{14}$ , (5) calculate the mean AOD over the area in question, and (6) investigate the relationship between AOD and  $\Delta T_{14}$ .

## 3. Results

Figure 2 shows RGB composite imagery of a subset of cloud clusters analyzed in the study. The red-green-blue (RGB) components are modulated by red =  $0.6\ \mu\text{m}$ , green =  $3.7\ \mu\text{m}$ , and blue =  $11\ \mu\text{m}$ . A maritime convective cloud cluster with an associated mean AOD = 0.1 is shown in Figure 2a. Figures 2b–2f show example cloud clusters over land with associated values of mean AOD = 0.2, 0.4, 0.5, 0.8, and 1.2, respectively.  $T$ - $r_e$  profiles for each case are shown in Figure 2g. At a given temperature, there is a decrease in  $r_e$  as the aerosol load increases. Most clouds have roughly the same  $T_{\text{base}}$ , i.e.,  $\sim 22^\circ\text{C}$ . Proceeding from clouds under clean conditions (Figure 2a) to clouds under successively more polluted conditions (Figures 2b–2f),  $T_{14}$  is  $20^\circ\text{C}$ ,  $12^\circ\text{C}$ ,  $-1^\circ\text{C}$ ,  $-4^\circ\text{C}$ ,  $-12^\circ\text{C}$ , and  $-24^\circ\text{C}$ , respectively. So for the maritime cloud case under clean conditions,  $\Delta T_{14} = 2^\circ\text{C}$ . For the other cloud cases which are under increasingly polluted conditions,  $\Delta T_{14} = 10^\circ\text{C}$ ,  $23^\circ\text{C}$ ,  $26^\circ\text{C}$ ,  $34^\circ\text{C}$ , and  $46^\circ\text{C}$ , respectively. Under polluted conditions, the onset of the warm rain process occurs higher in the atmosphere.

The extent of suppression of warm rain by aerosols in convective clouds is parameterized using the dependence of  $\Delta T_{14}$  on AOD. The effect of aerosols on cloud microphysical properties is manifested by a decrease in  $r_e$  and an increase in  $\Delta T_{14}$  as aerosol loading increases. Figure 3 shows that  $\Delta T_{14}$  is positively correlated with AOD, which rounded to the nearest one tenth. When the AOD increases by one unit,  $\Delta T_{14}$  increases by  $37^\circ\text{C}$ . Assuming a moist adiabatic lapse rate of  $6.5^\circ\text{C km}^{-1}$ , this suggests that warm rain

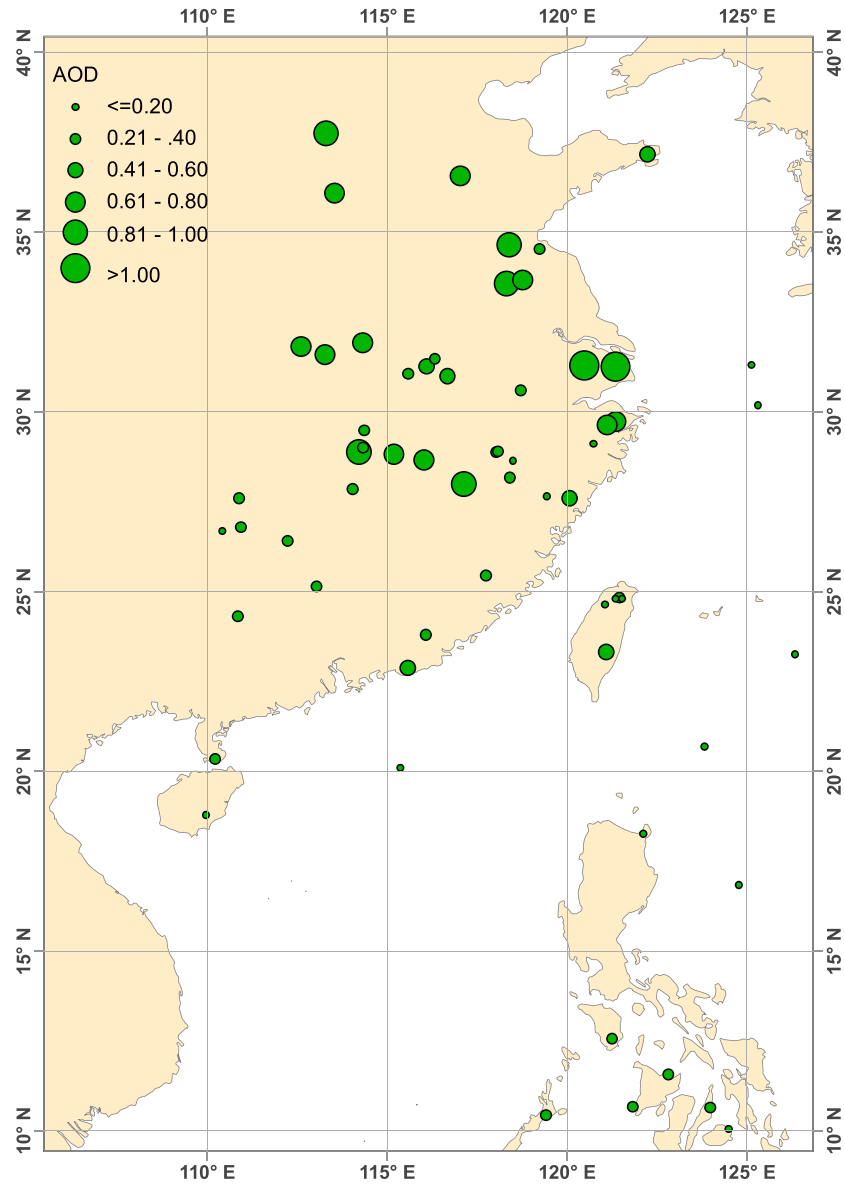


**Figure 1.** Geographical locations of the 64 cloud clusters analyzed in this study. The size of the mark is proportional to the mean AOD retrieved in the vicinity of the cloud cluster.

formation is delayed by  $\sim 5.5$  km.  $\Delta T_{14}$  is less than  $25^\circ\text{C}$  when  $\text{AOD} \leq 0.5$ . Almost all cases considered here have  $\Delta T_{14}$  ranging from  $20^\circ\text{C}$  to  $60^\circ\text{C}$  when  $\text{AOD} > 0.5$ .

#### 4. Potential Artifacts

##### 4.1. Effect of Cloud Fraction

Recent studies have demonstrated the challenges that arise when retrieving aerosol properties near clouds. Chand *et al.* [2012] found a 25% enhancement in AOD when the CF ranged from 0.1–0.2 to 0.8–0.9. The aerosol humidification effect can explain about a quarter of the correlation between cloud cover and AOD [Jeong and Li, 2010]. Redemann *et al.* [2009] found that in 75% of the cases they considered, there was an increase of up to 20% in AOD within the closest 2 km near clouds. It is then useful to test if and how much cloud thickness and CF affect AOD and its correlation with  $\Delta T_{14}$ .

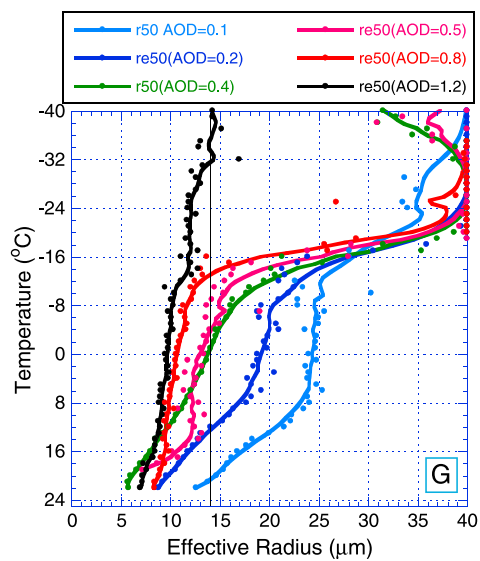
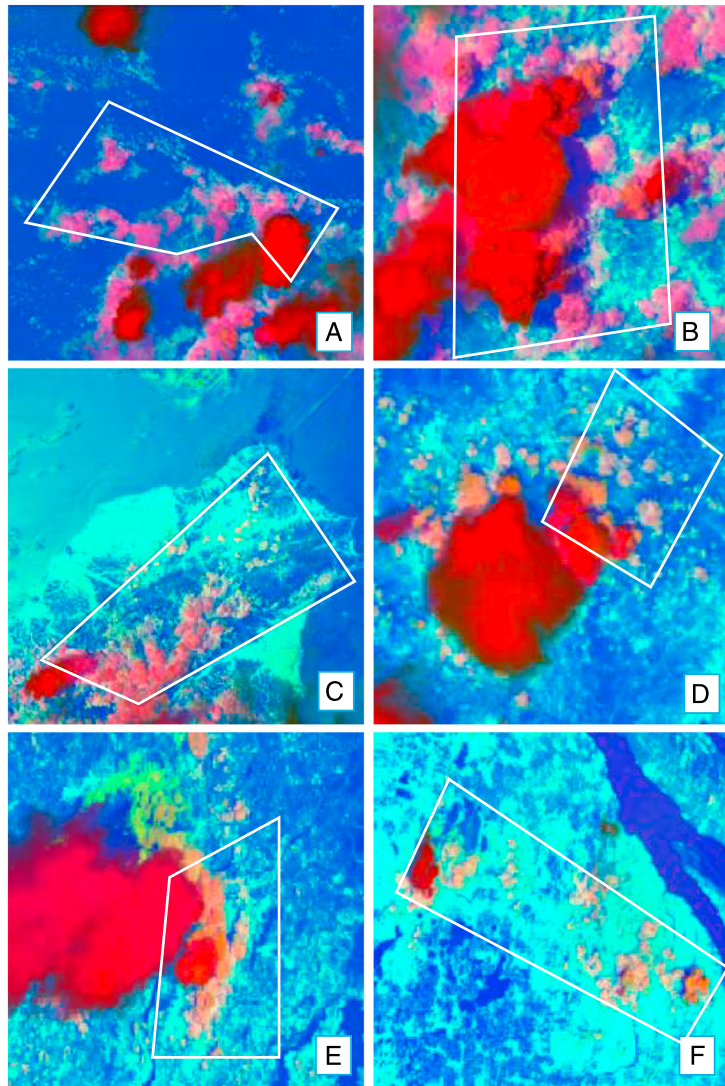
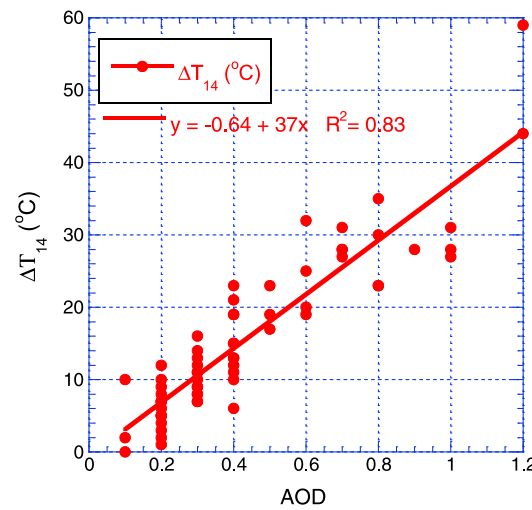


Figure 2



**Figure 3.**  $\Delta T_{14}$  as a function of AOD (rounded to the nearest one tenth) for all cases considered here. The red line is the linear regression line through the points.

Data were divided into two categories according to  $T_{top}$  and CF. For all cases selected,  $T_{top}$  ranges from 7°C to  $-83^{\circ}\text{C}$  and CF ranges from 0.01 to 0.29. The selection of cases with relatively small CFs helps to eliminate/reduce the retrieval error in AOD. Figure 4 shows  $\Delta T_{14}$  as a function of MODIS-retrieved AOD when the data are divided according to  $T_{top}$  ( $T_{top} < -40^{\circ}\text{C}$  and  $T_{top} \geq -40^{\circ}\text{C}$ ; Figure 4a) and according to CF ( $\text{CF} < 0.1$  and  $\text{CF} \geq 0.1$ ; Figure 4b). The relationships between MODIS- and VIIRS-retrieved AOD are shown in Figure 4c. Validations of the VIIRS AOD data showed somewhat inferior quality than the MODIS AOD data over land [Jackson et al., 2013; Liu et al., 2014], but the two products have a reasonable agreement only for 2013, as is shown in Figure 4c. Therefore, we repeated in Figure 4d the analysis shown in Figure 4b but with VIIRS AOD from 2013 only. Qualitatively, the results of the VIIRS AOD (Figure 4d) are similar to those

derived from MODIS AOD (Figure 4b) but with somewhat larger scattering. According to the official website, VIIRS aerosol AOD product available is still at Beta Maturity Status from 2 May 2012 to 22 January 2013. As such, we employ the MODIS AOD for the main analysis in this study.

The linear relationships for data sets of different  $T_{top}$  are similar (Figure 4a). This implies that cloud thickness has a negligible effect on the relationship between  $\Delta T_{14}$  and AOD. This may be because the clouds in the scenes selected are distant enough from each other to the point that they have little effect on AOD retrievals by reflected solar radiation from their sides. Concerning CF, about 50% of the cloud cluster cases have a CF value  $< 0.1$  within the area that AOD was retrieved. The correlation between  $\Delta T_{14}$  and AOD is weaker when  $\text{CF} > 0.1$  than when  $\text{CF} < 0.1$ , especially when AOD is large (Figures 4b and 4d). It is possible that AOD is overestimated when CF becomes larger, but such an effect is not evident for  $\text{AOD} < 0.6$ . At  $\text{AOD} > 0.6$   $\Delta T_{14}$  does not increase as much with further increase in AOD. The possible causes for that will be discussed in section 5.

#### 4.2. The Effect of Solar Scattering Angle

Satellite-retrieved  $r_e$  can be biased due to the three-dimensional geometry of convective clouds [Vant-Hull et al., 2007]. The illuminated side of clouds causes an underestimation in  $r_e$  when not accounting for the orientation of the cloud surface from horizontal. On the other hand, a large overestimation of  $r_e$  occurs for convective clouds to the west of the nadir that are self-shadowed [Vant-Hull et al., 2007]. Marshak et al. [2006] have analyzed broken cumulus cloud fields using MODIS and Advanced Spaceborne Thermal Emission and Reflection Radiometer data and recommend against blindly using retrieved  $r_e$  for this kind of cloud field because  $r_e$  is larger for shadowed clouds than for illuminated clouds. Figure 5 illustrates the geometry of satellite, the Sun, and cloud scenes under observation.

To evaluate this effect, data were divided into five categories according to scattering angle (Figure 5), from the shadowed clouds to the west of the nadir, up to  $-34^{\circ}$ , to the sunny sides of clouds, as seen with satellite zenith angle up to  $40^{\circ}$  on the east of the nadir. The shadowed clouds have smaller  $\Delta T_{14}$  compared with the clouds in the sunny side ((Figure 6a) all the data and (Figure 6b) the data with  $\text{CF} < 0.1$ ). This

**Figure 2.** Microphysics RGB composite imagery (red =  $0.6 \mu\text{m}$ , green =  $3.7 \mu\text{m}$ , and blue =  $11 \mu\text{m}$ ) showing a subset of cloud cluster cases considered in the study: (a) at 05:12 UT, 25 August 2013, centered on  $20.61^{\circ}\text{N}$ ,  $121.08^{\circ}\text{E}$ ; (b) 05:27 UT, 30 June 2014, centered on  $23.70^{\circ}\text{N}$ ,  $116.10^{\circ}\text{E}$ ; (c) 05:01 UT, 30 July 2013, centered on  $24.83^{\circ}\text{N}$ ,  $121.46^{\circ}\text{E}$ ; (d) 05:13 UT, 09 August 2013, centered on  $27.59^{\circ}\text{N}$ ,  $120.08^{\circ}\text{E}$ ; (e) 05:37 UT, 12 July 2013, centered on  $28.66^{\circ}\text{N}$ ,  $116.02^{\circ}\text{E}$ ; and (f) 05:13 UT, 09 August 2013, centered on  $31.28^{\circ}\text{N}$ ,  $121.09^{\circ}\text{E}$ . (g)  $T-r_e$  profiles under different aerosol loading conditions for the cloud clusters seen in Figures 2a–2f. The 50th percentiles of  $r_e$  for any given  $T$  are plotted as the smooth interpolation shows.

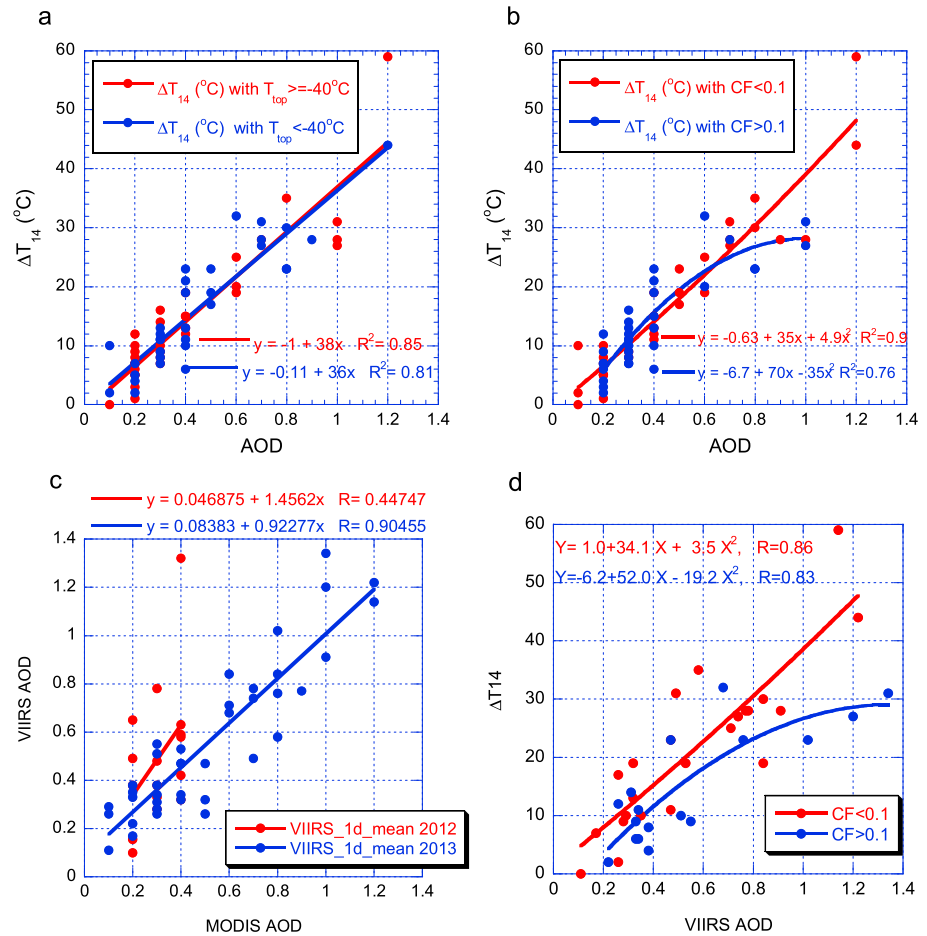


**Figure 4.**  $\Delta T_{14}$  as a function of AOD where data are divided according to (a)  $T_{top}$  and (b) CF. The blue and red markers in Figure 4a represent data associated with  $T_{top} < -40^\circ\text{C}$  and  $T_{top} \geq -40^\circ\text{C}$ , respectively. The blue and red markers in Figure 4b represent data associated with  $CF > 0.1$  and  $CF < 0.1$ , respectively. Color-coded linear regression lines in Figure 4a and polynomial regression lines in Figure 4b are shown. (c) The relationships between MODIS- and VIIRS-retrieved AOD for 2012 (red) and 2013 (blue). (d) The same as in Figure 4b but for VIIRS AOD from 2013.

means that satellite-retrieved  $r_e$  for shadowed clouds reach  $14 \mu\text{m}$  earlier, i.e., at warmer temperatures, than those for backscattering clouds. Comparing Figure 6a with Figure 6b, when  $CF < 0.1$ , we find that the spread is somewhat smaller and the correlations are higher. The possible reasons will be discussed in section 5.

### 5. Possible Causes and Effects of the $\Delta T$ -AOD Relationships

The obtained AOD- $\Delta T_{14}$  relationships are remarkably linear. The linearity resembles the linearity between numbers of activated CCN into cloud droplets at cloud base ( $N_a$ ) and  $D_p$  [Freud and Rosenfeld, 2012]. It is commonly accepted that a higher AOD is associated with larger CCN concentrations [Andreae, 2009], and therefore, as long as AOD is linearly correlated with CCN, we should expect similarly linear relationships between AOD and  $D_p$ . The  $N_a$ - $D_p$  relationship is linear as long as a similar amount of water vapor is condensed for a given increase in height of the rising cloud parcel. At greater heights, the rate of increase in  $r_e$  with height becomes smaller [Freud and Rosenfeld, 2012]. This trend is compensated by the fact that  $dN_a/d\text{CCN}$  decreases when CCN concentration becomes very large and a transition occurs for the cloud drop nucleation from aerosol limited to updraft limited [Reutter et al., 2009]. The combination of these two opposite effects likely keeps the AOD- $\Delta T_{14}$  relationships linear.

According to Figure 4b the AOD- $\Delta T_{14}$  relationship is linear for cases with  $CF < 0.1$ , but when  $CF > 0.1$ , the AOD can increase beyond the linear relationship (not always) for deep clouds, which means that  $\Delta T_{14}/\text{AOD}$

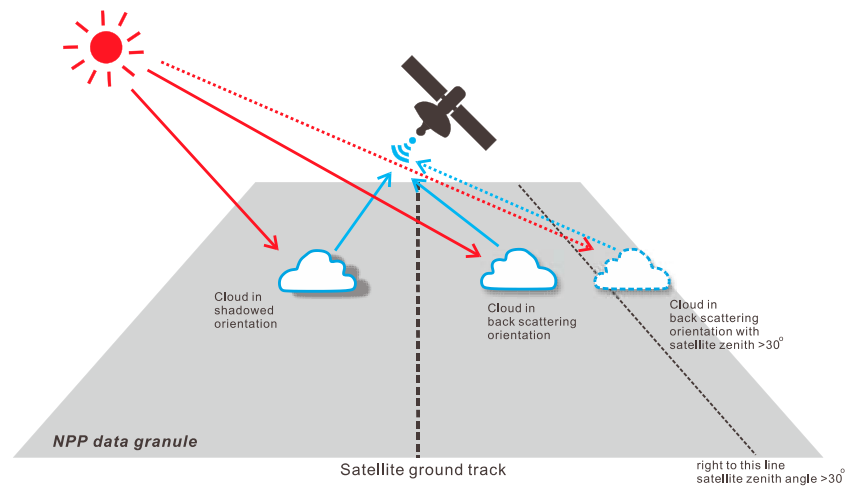


**Figure 5.** Geometries of shadowing and illumination with respect to convective clouds. The satellite views the shadowed side of a cloud to the left of the ground track, backscattered reflection from the cloud in the center, and the illuminated side of the cloud to the right of the ground track (adapted from Vant-Hull et al. [2007]).

is smaller, especially for the larger values of  $\Delta T_{14}$ . This might be caused by the possibility that the increased AOD for larger  $\Delta T_{14}$  is contributed by a larger depth of the aerosol layer instead of a greater concentration of aerosols at a fixed depth above the surface. This can be a result of the fact that a cloud droplet that was nucleated on an aerosol particle in the cloud base is not likely to coalesce into raindrop or accrete to an ice hydrometeor below the height of rain initiation. All cloud drops that do not form precipitation eventually must evaporated and release the CCN on which they were nucleated back to the ambient air. This is most likely to happen by mixing from the side of the cloud below the height of rain initiation. In such case the CCN that nucleated the cloud droplet is released back into the cloud-free air at a level anywhere between the cloud base and the height of rain initiation. This means that a larger  $\Delta T_{14}$  can increase the depth of the layer that contains aerosols that originate from the boundary layer, thus increasing AOD without a necessary respective increase with aerosol concentrations at the boundary layer. This can cause a greater AOD for the same CCN or for the same  $\Delta T_{14}$ . A larger CF of deep clouds means a greater vertical convective mass flux and a, respectively, greater transport and detrainment of more aerosols aloft. This is consistent with the line for  $CF > 0.1$  in Figure 4b.

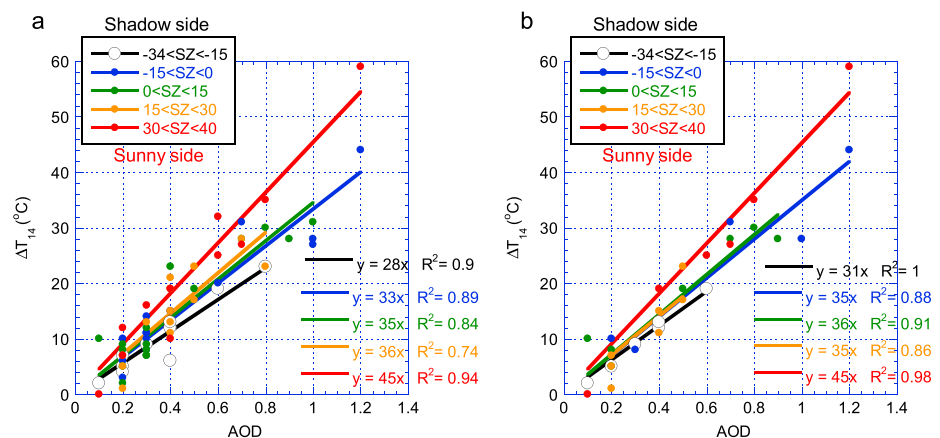


**Figure 6.**  $\Delta T_{14}$  as a function of AOD where data are divided according to satellite zenith angle, (a) for all the data and (b) for the data associated with  $CF < 0.1$ . The regression lines are forced through the origin.

## 6. Summary and Conclusions

The suppression of warm rain by aerosols has been recognized mainly through their impact on cloud droplet size and the suppression of droplet coalescence. Previous studies of this topic have been based on either aircraft measurements or model simulations. With the advent of high-resolution sensor of the VIIRS imager,  $T_{\text{base}}$  of convective clouds and the vertical evolution of their cloud droplet  $r_e$  can now be retrieved more accurately [Zhu *et al.*, 2014; Rosenfeld *et al.*, 2014b]. This made the present study possible. It demonstrates that for convective clouds in the developing stage, cloud droplet size increases with height, but the rate of change varies with aerosol loading, i.e., faster under clean than under dirty conditions. For a cloud to reach the critical size necessary to rain, it must develop to a certain thickness  $D_p$  or to a certain cloud top temperature, whose threshold values depend on AOD. The temperature difference between  $T_{\text{base}}$  and the critical cloud top temperature for rain initiation as determined by  $r_e$  exceeding  $14\ \mu\text{m}$  ( $\Delta T_{14}$ ) can thus serve as another measure of aerosol-cloud-precipitation interactions. Convective cloud scenes over Southeast Asia were identified and selected for further study.

The  $\Delta T_{14}$  and AOD are positively correlated ( $R^2 = 0.83$ ). A unit increase in AOD delays warm rain initiation by  $D_p$  of about 5.5 km over the study area. The AOD- $\Delta T_{14}$  relationship is subject to uncertainties due to some inherent satellite retrieval errors. The three-dimensional structure of convective clouds may bias the retrieved  $r_e$ . The assumption that AOD corresponds to aerosol concentrations may be erroneous too. The retrieval errors and their impact on the AOD- $\Delta T_{14}$  relationship were evaluated.

The impact of viewing geometry on the indicated AOD- $\Delta T_{14}$  relationships was evaluated. Because cloud droplet size tends to be overestimated when clouds are partly shaded, the AOD- $\Delta T_{14}$  relationship shows a systematic dependence on viewing geometry. The indicated  $r_e$  is larger at the angles where the satellite views the partly shaded side of the clouds at the same AOD and is lower at the sunny sides of the clouds.

Another source of error is the possible impact of  $\Delta T_{14}$  on AOD. A larger  $\Delta T_{14}$  means that rain is suppressed to greater heights in the clouds, respectively, suppressing the wet scavenging of the aerosols that were ingested into the cloud. Instead, the mixing and evaporating of the cloud with the ambient air releases back the aerosols aloft, which contribute to increasing AOD without a respective increase in aerosol concentrations below cloud base. This is indicated by the decrease of the slope of the AOD- $\Delta T_{14}$  relationships when  $\text{CF} > 0.1$  and  $\Delta T_{14} > \sim 20^\circ\text{C}$ .

Despite the problems in using AOD as a proxy of CCN [Liu and Li, 2014], the AOD seems to be a useful surrogate for CCN under the special conditions which are identified here. The AOD- $\Delta T_{14}$  relationships, after accounting for some of the measurement artifacts, behave in agreement with the way that  $\Delta T_{14}$  is expected to vary with CCN concentrations. The existence of such tight AOD- $\Delta T_{14}$  relationships over a wide range of meteorological conditions indicates that CCN dominates the  $T$ - $r_e$  relationships up to the height where precipitation initiates, because the condensational growth rate of  $r_e$  with height is not affected by the updraft speeds well above cloud base but rather by the number of CCN that were activated into cloud drops at cloud base. Above that height,  $r_e$  grows more slowly with height for greater updrafts [Rosenfeld *et al.*, 2008b]. This is a simple and powerful relationship that can be used for parameterization of the effect of AOD on cloud microstructure and precipitation-forming processes. Furthermore, under some conditions (when  $r_e$  exceeds  $12\ \mu\text{m}$  at  $T > -5^\circ\text{C}$ ), the  $T$ - $r_e$  relationships can affect cloud glaciation temperature and ice particle size in the anvils even more than ice nuclei concentrations do [Rosenfeld *et al.*, 2011; Jiang *et al.*, 2011].

### Acknowledgments

We thank the anonymous reviewers for their helpful suggestions. This research was supported by the National Basic Program of China (973 Program, 2013CB955804) and the China Special Fund for Meteorological Research in the Public Interest (GYHY201306005). The NPP/VIIRS imager and MODIS AOD data are obtained from <http://www.class.ngdc.noaa.gov/> and <http://disc.sci.gsfc.nasa.gov/giovanni>, respectively. The retrieved  $T$ - $r_e$  profiles and other relevant data will be made available upon request (contact: Yannian Zhu, yannian.zhu@yahoo.com).

### References

- Andreae, M. O. (2009), Correlation between cloud condensation nuclei concentration and aerosol optical thickness in remote and polluted regions, *Atmos. Chem. Phys.*, 9, 543–556, doi:10.5194/acp-9-543-2009.
- Andreae, M. O., and D. Rosenfeld (2008), Aerosol–cloud–precipitation interactions. Part 1. The nature and sources of cloud-active aerosols, *Earth Sci. Res.*, 89(1–2), 13–41, doi:10.1016/j.earscirev.2008.03.001.
- Andreae, M. O., D. Rosenfeld, P. Artaxo, A. A. Costa, G. P. Frank, K. M. Longo, and M. A. Silva-Dias (2004), Smoking rain clouds over the Amazon, *Science*, 303(5662), 1337–1342.

- Chand, D., R. Wood, S. J. Ghan, M. Wang, M. Ovchinnikov, P. J. Rasch, S. Miller, B. Schichtel, and T. Moore (2012), Aerosol optical depth increase in partly cloudy conditions, *J. Geophys. Res.*, *117*, D17207, doi:10.1029/2012JD017894.
- Feingold, G., W. Cotton, S. Kreidenweis, and J. Davis (1999), The impact of giant cloud condensation nuclei on drizzle formation in stratocumulus: Implications for cloud radiative properties, *J. Atmos. Sci.*, *56*(24), 4100–4117.
- Freud, E., and D. Rosenfeld (2012), Linear relation between convective cloud drop number concentration and depth for rain initiation, *J. Geophys. Res.*, *117*, D02207, doi:10.1029/2011JD016457.
- Freud, E., D. Rosenfeld, and J. R. Kulkarni (2011), Resolving both entrainment-mixing and number of activated CCN in deep convective clouds, *Atmos. Chem. Phys.*, *11*, 12,887–12,900, doi:10.5194/acp-11-12887-2011.
- Jackson, J., H. Liu, I. Laszlo, S. Kondragunta, L. A. Remer, J. Huang, and H.-C. Huang (2013), Suomi-NPP VIIRS aerosol algorithms and data products, *J. Geophys. Res. Atmos.*, *118*, 12,673–12,689, doi:10.1002/2013JD020449.
- Jeong, M.-J., and Z. Li (2010), Separating real and apparent effects of cloud, humidity, and dynamics on aerosol optical thickness near cloud edges, *J. Geophys. Res.*, *115*, D00K32, doi:10.1029/2009JD013547.
- Jiang, J. H., H. Su, M. R. Schoeberl, S. T. Massie, P. Colarco, S. Platnick, and N. J. Livesey (2008), Clean and polluted clouds: Relationships among pollution, ice clouds, and precipitation in South America, *Geophys. Res. Lett.*, *35*, L14804, doi:10.1029/2008GL034631.
- Jiang, J. H., H. Su, C. Zhai, S. T. Massie, M. R. Schoeberl, P. R. Colarco, S. Platnick, Y. Gu, and K. N. Liou (2011), Influence of convection and aerosol pollution on ice cloud particle effective radius, *Atmos. Chem. Phys.*, *11*, 457–463, doi:10.5194/acp-11-457-2011.
- Jones, T. A., and S. A. Christopher (2010), Statistical properties of aerosol-cloud-precipitation interactions in South America, *Atmos. Chem. Phys.*, *10*(5), 2287–2305, doi:10.5194/acp-10-2287-2010.
- Konwar, M., R. S. Mahes Kumar, J. R. Kulkarni, E. Freud, B. N. Goswami, and D. Rosenfeld (2012), Aerosol control on depth of warm rain in convective clouds, *J. Geophys. Res.*, *117*, D13204, doi:10.1029/2012JD017585.
- Koren, I., O. Altaratz, L. A. Remer, G. Feingold, J. V. Martins, and R. H. Heiblum (2012), Aerosol-induced intensification of rain from the tropics to the mid-latitudes, *Nat. Geosci.*, *5*(2), 118–122, doi:10.1038/ngeo1364.
- Lensky, I. M., and D. Rosenfeld (2006), The time-space exchangeability of satellite retrieved relations between cloud top temperature and particle effective radius, *Atmos. Chem. Phys.*, *6*, 2887–2894.
- Li, Z., F. Niu, J. Fan, Y. Liu, D. Rosenfeld, and Y. Ding (2011), Long-term impacts of aerosols on the vertical development of clouds and precipitation, *Nat. Geosci.*, *4*, 888–894.
- Lin, J. C., T. Matsui, R. A. Pielke Sr., and C. Kummerow (2006), Effects of biomass-burning-derived aerosols on precipitation and clouds in the Amazon Basin: A satellite-based empirical study, *J. Geophys. Res.*, *111*, D19204, doi:10.1029/2005JD006884.
- Liu, H., L. A. Remer, J. Huang, H. C. Huang, S. Kondragunta, I. Laszlo, M. Oo, and J. M. Jackson (2014), Preliminary evaluation of S-NPP VIIRS aerosol optical thickness, *J. Geophys. Res. Atmos.*, *119*, 3942–3962, doi:10.1002/2013JD020360.
- Liu, J., and Z. Li (2014), Estimation of cloud condensation nuclei concentration from aerosol optical quantities: Influential factors and uncertainties, *Atmos. Chem. Phys.*, *14*, 471–483, doi:10.5194/acp-14-471-2014.
- Marshak, A., S. Platnick, T. Várnai, G. Wen, and R. F. Cahalan (2006), Impact of three-dimensional radiative effects on satellite retrievals of cloud droplet sizes, *J. Geophys. Res.*, *111*, D09207, doi:10.1029/2005JD006686.
- Martins, J. A., M. A. F. Silva Dias, and F. L. T. Gonçalves (2009), Impact of biomass burning aerosols on precipitation in the Amazon: A modeling case study, *J. Geophys. Res.*, *114*, D02207, doi:10.1029/2007JD009587.
- Posselt, R., and U. Lohmann (2008), Influence of giant CCN on warm rain processes in the ECHAM5 GCM, *Atmos. Chem. Phys.*, *8*, 3769–3788, doi:10.5194/acp-8-3769-2008.
- Redemann, J., Q. Zhang, P. B. Russell, J. M. Livingston, and L. A. Remer (2009), Case studies of aerosol remote sensing in the vicinity of clouds, *J. Geophys. Res.*, *114*, D06209, doi:10.1029/2008JD010774.
- Reutter, P., H. Su, J. Trentmann, M. Simmel, D. Rose, S. S. Gunthe, H. Wernli, M. O. Andreae, and U. Pöschl (2009), Aerosol- and updraft-limited regimes of cloud droplet formation: Influence of particle number, size and hygroscopicity on the activation of cloud condensation nuclei (CCN), *Atmos. Chem. Phys.*, *9*, 7067–7080, doi:10.5194/acp-9-7067-2009.
- Rosenfeld, D. (1999), TRMM observed first direct evidence of smoke from forest fires inhibiting rainfall, *Geophys. Res. Lett.*, *26*(20), 3105–3108, doi:10.1029/1999GL006066.
- Rosenfeld, D. (2000), Suppression of rain and snow by urban and industrial air pollution, *Science*, *287*, 1793–1796.
- Rosenfeld, D., and G. Gutman (1994), Retrieving microphysical properties near the tops of potential rain clouds by multispectral analysis of AVHRR data, *Atmos. Res.*, *34*(1–4), 259–283.
- Rosenfeld, D., and I. M. Lensky (1998), Satellite-based insights into precipitation formation processes in continental and maritime convective clouds, *Bull. Am. Meteorol. Soc.*, *79*, 2457–2476.
- Rosenfeld, D., and W. Woodley (2003), Closing the 50-year circle: From cloud seeding to space and back to climate change through precipitation physics, *Meteorol. Monogr.*, *51*, 59–80.
- Rosenfeld, D., U. Lohmann, G. B. Raga, C. D. O'Dowd, M. Kulmala, S. Fuzzi, A. Reissell, and M. O. Andreae (2008a), Flood or drought: How do aerosols affect precipitation?, *Science*, *321*(5894), 1309–1313.
- Rosenfeld, D., W. L. Woodley, A. Lerner, G. Kelman, and D. T. Lindsey (2008b), Satellite detection of severe convective storms by their retrieved vertical profiles of cloud particle effective radius and thermodynamic phase, *J. Geophys. Res.*, *113*, D04208, doi:10.1029/2007JD008600.
- Rosenfeld, D., X. Yu, G. Liu, X. Xu, Y. Zhu, Z. Yue, J. Dai, Z. Dong, Y. Dong, and Y. Peng (2011), Glaciation temperatures of convective clouds ingesting desert dust, air pollution and smoke from forest fires, *Geophys. Res. Lett.*, *38*, L21804, doi:10.1029/2011GL049423.
- Rosenfeld, D., H. Wang, and P. J. Rasch (2012), The roles of cloud drop effective radius and LWP in determining rain properties in marine stratocumulus, *Geophys. Res. Lett.*, *39*, L13801, doi:10.1029/2012GL052028.
- Rosenfeld, D., B. Fishman, Y. Zheng, T. Goren, and D. Giguzin (2014a), Combined satellite and radar retrievals of drop concentration and CCN at convective cloud base, *Geophys. Res. Lett.*, *41*, 3259–3265, doi:10.1002/2014GL059453.
- Rosenfeld, D., G. Liu, X. Yu, Y. Zhu, J. Dai, X. Xu, and Z. Yue (2014b), High-resolution (375 m) cloud microstructure as seen from the NPP/VIIRS satellite imager, *Atmos. Chem. Phys.*, *14*, 2479–2496, doi:10.5194/acp-14-2479-2014.
- Sullivan, J., C. Walton, J. Brown, and R. Evans (1993), Nonlinearity corrections for the thermal infrared channels of the Advanced Very High Resolution Radiometer: Assessment and recommendations, *NOAA Tech. Rep. NESDIS*, *69*, 31 pp.
- Suzuki, K., T. Y. Nakajima, and G. L. Stephens (2010), Particle growth and drop collection efficiency of warm clouds as inferred from joint CloudSat and MODIS observations, *J. Atmos. Sci.*, *67*, 3019–3032, doi:10.1175/2010JAS3463.1.
- Tao, W.-K., J.-P. Chen, Z. Li, C. Wang, and C. Zhang (2012), Impact of aerosols on convective clouds and precipitation, *Rev. Geophys.*, *50*, RG2001, doi:10.1029/2011RG000369.

- Teller, A., and Z. Levin (2006), The effects of aerosols on precipitation and dimensions of subtropical clouds: A sensitivity study using a numerical cloud model, *Atmos. Chem. Phys.*, *6*(1), 67–80, doi:10.5194/acp-6-67-2006.
- Vant-Hull, B., A. Marshak, L. A. Remer, and Z. Li (2007), The effects of scattering angle and cumulus cloud geometry on satellite retrievals of cloud droplet effective radius, *IEEE Trans. Geosci. Remote Sens.*, *45*(4), 1039–1045.
- Yan, H., Z. Li, J. Huang, M. Cribb, and J. Liu (2014), Long-term aerosol-mediated changes in cloud radiative forcing of deep clouds at the top and bottom of the atmosphere over the Southern Great Plains, *Atmos. Chem. Phys.*, *14*(14), 7113–7124, doi:10.5194/acp-14-7113-2014.
- Zhu, Y., D. Rosenfeld, X. Yu, G. Liu, J. Dai, and X. Xu (2014), Satellite retrieval of convective cloud base temperature based on the NPP/VIIRS imager, *Geophys. Res. Lett.*, *41*, 1308–1313, doi:10.1002/2013GL058970.